Chinese Science Bulletin

Low-field positive and high-field negative magnetoresistances in multiphase Fe-oxide thin films at room temperature

ZHAO Kun[1,3†], XING Jie[2], LIU YuZi[2], ZHAO JianGao[2] & LÜ HuiBin[2]

[1] Department of Mathematics and Physics, China University of Petroleum, Beijing 102249, China;
[2] Beijing National Laboratory for Condensed Matter Physics, Institute of Physics, Chinese Academy of Sciences, Beijing 100080, China;
[3] International Center for Materials Physics, Chinese Academy of Sciences, Shenyang 110016, China

Multiphase Fe-oxide thin films are fabricated on glass substrates by a facing-target sputtering technique. X-ray diffraction and X-ray photoelectron spectroscopy reveal that Fe, Fe_3O_4, γ-Fe_2O_3 and FeO coexist in the films. High resolution transmission electron microscopy shows the well-defined columnar grain structure with the unoxidized Fe as the core and iron-oxide as the shell. The low-field positive and high-field negative magnetoresistances coexist in such a system at room temperature, which can be explained by considering a shell/core model. Nonlinear current-voltage curve and photovoltaic effect further confirm the tunneling-type conduction.

magnetoresistance, magnetic properties, thin film

Core-shell composite materials and hollow capsules have attracted a great deal of interest due to their versatile structures and properties for many significant applications[1−10]. A prominent example is iron-iron oxide system which includes many phases, such as Fe_3O_4, γ-Fe_2O_3, α-Fe_2O_3 and FeO_{1-x}. Gangopadhyay et al.[11] attributed the enhancement in coercivity of fine iron particles to a core-shell type of structure, where the core consisted of metallic Fe and the shell was composed of Fe oxides. Prados et al.[12] studied the magnetic behavior of exchange-coupled passivated Fe nanoparticles with the structure modification of the Fe-oxide shell, and a decrease of the strength of the exchange anisotropy was observed as the external oxide shell was ordered. Recently Rybchenko et al.[13] demonstrated that low-field magnetoresistance in granular magnetite could be essentially enhanced by the passivation of the grain's interface.

Previously, we have prepared single-phase Fe_3O_4 thin film and found a huge negative magnetoresistance (MR) of ~ –27% at room temperature, which was attributed to the spin-polarized intergrain tunneling through the grain boundaries[14]. In this paper, attention is focused on the low field positive and high-field negative MR of a system consisting of multiphase Fe-oxide at room temperature. Here, MR ratio is defined as $(R_{4\ \mathrm{kOe}}-R_H)/R_{4\ \mathrm{kOe}}$, where R_H is the resistance in the applied magnetic field H (< 4 kOe), since the magnetization appears to be saturated at H = 4 kOe based on our magnetization measurement.

1 Experiment

A 100-nm-thick Fe metal film was deposited on glass substrate at a sputtering rate of 0.092 nm/s by a facing-target sputtering technique[14−16]. Then the Fe film was subjected to *in situ* plasma oxidation with a power of 40 W at about 200℃, which was different from that in ref. [14], in an oxygen atmosphere of 8 Pa for 400 s. Following oxidation, the film was cooled to room temperature in a vacuum of 2×10^{-3} Pa. X-ray diffraction

(XRD) analysis of the as-prepared sample revealed the presence of Fe and its oxides as shown in Figure 1. The peaks at 43.0° and 57.3° can be deconvoluted into Fe_3O_4 and γ-Fe_2O_3 components. The other small peaks may come from non-stoichiometric FeO. Different from the XRD result of single-phase Fe_3O_4 film[14], it is obvious that the present Fe-oxide film is incompletely oxidized since the oxidizing time is insufficient and the heating temperature is lower.

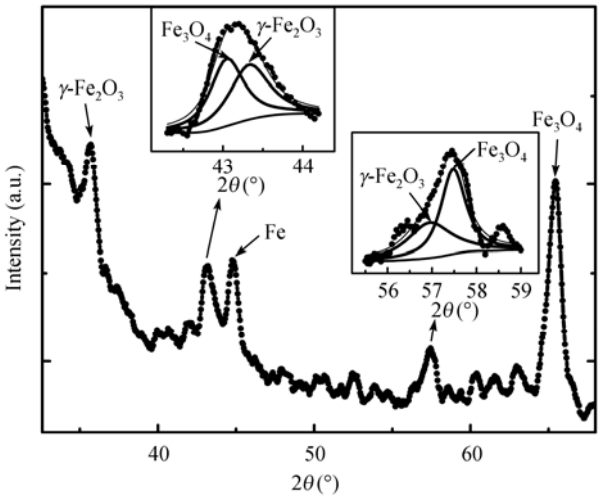

Figure 1 XRD pattern for the Fe-oxide thin film grown on glass substrate. The insets show the deconvolution of the peaks at 43.0° and 57.3°, respectively.

2 Results and discussion

The presence of oxide species was also fully confirmed by X-ray photoelectron spectroscopy (XPS). A typical XPS spectrum at etching depths of 20 nm is shown in Figure 2. The position of the Fe oxides as marked in the spectrum was obtained by deconvoluting the asymmetric broadening of the higher energy edge of the metallic Fe peak. The chemical composition was determined from the relative intensities of Fe and Fe-oxide peaks in the XPS spectrum, and was found to be about 37.5% Fe, 29.7% Fe_3O_4, 19.3% FeO, and 13.5% γ-Fe_2O_3. Further confirmation of the sample growth has been obtained from microstructure investigations of the films using high-resolution transmission electron microscopy (HRTEM). Figure 3 shows a cross-sectional HRTEM image of a typical Fe-oxide film. An arrayed columnar structure is formed with clear boundaries between grains, and the column diameter remains relatively constant.

From the above results, we infer the oxidation process of the sample as follows. During the process of plasma

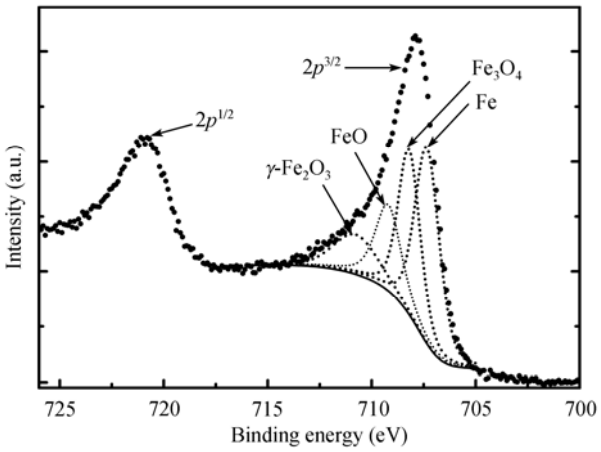

Figure 2 2*p* XPS of a typical Fe-oxide film at the etching depth of 20 nm, showing the presence of metallic Fe and its oxides.

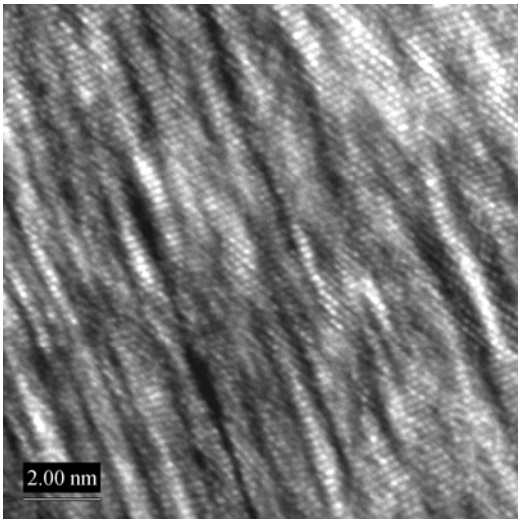

Figure 3 HRTEM of a cross-sectional image of a typical Fe-oxide thin film.

oxidation, oxygen atoms collected on the surface of the film are chemisorbed on the surface Fe crystal grains, where lattice defects and vacancies are abundant, and fill up these vacancies to form unstable nonstoichiometric Fe-O "compounds". They are reorganized subsequently under the action of chemical bonding force into regular and stable Fe oxides: Fe_3O_4, FeO, and γ-Fe_2O_3. The re-orientation of atoms may introduce new lattice defects near the grain boundaries, which prompts the O to diffuse into the oxide shells with growing thickness. Thus the unoxidized Fe is left as the core, and the core-shell morphology of the columnar grain is formed at the termination of oxidation process.

Figure 4 is a typical magnetic hysteresis loop from an unpatterned film measured at room temperature with the

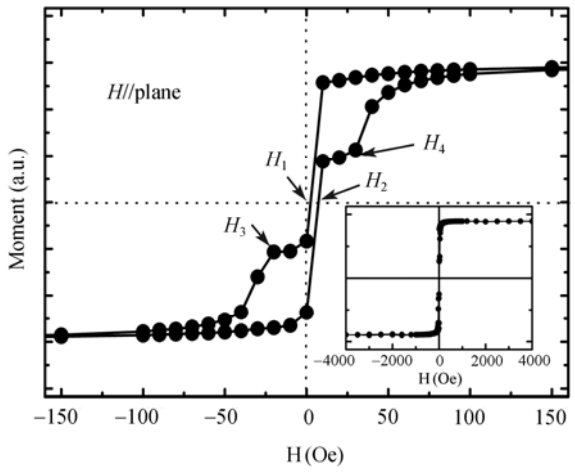

Figure 4 The blowup of the low field part of the magnetic hysteresis loop for an unpatterned Fe-oxide thin film at room temperature. The inset shows the whole hysteresis curve. The magnetic field was applied in the film plane.

magnetic field applied in the film plane using the vibrating sample magnetometer (VSM). The macroscopic loop is the composition of the hysteresis of all individual particles. In general, two materials, each having a conventional hysteresis loop with different coercivities, will produce a wasp-waist loop when coupled[17]. The present loop shows four field-selected parameters: H_1 = 2.4 Oe, H_2 = 7.4 Oe, H_3 = –21.4 Oe, and H_4 = 29.8 Oe. Thus, two coercivity fields can be obtained, $H_{c1} = (H_2–H_1)/2$ = 2.5 Oe and $H_{c2} = (H_4–H_3)/2$ = 25.9 Oe. The coercivity difference and wasp-waist of the loop create well-defined parallel and antiparallel states between the Fe-core and oxide-shell.

The films are patterned into strips of 0.5 mm in width and 4.5 mm in length using optical lithography and Ar ion-beam etching for four-probe transport measurements. The distance between probes was fixed at about 1.5 mm, and the applied field H was in the film plane and parallel to the current direction which was also in the film plane.

The field dependence of the room-temperature resistance for the strip is shown in Figure 5. The fields, at which the resistance changes abruptly, do not match exactly with the result of VSM because the MR is measured after the lithography process. Nevertheless, the MR change due to the magnetization reversal can be seen clearly for H < 1 kOe as shown in Figure 5(a). At H > 150 Oe, when the moments of the adjacent core and shell are aligned along the field direction and parallel to each other, R attains a high value. Whereas, in between the coercive fields for the core and shell, R reaches the

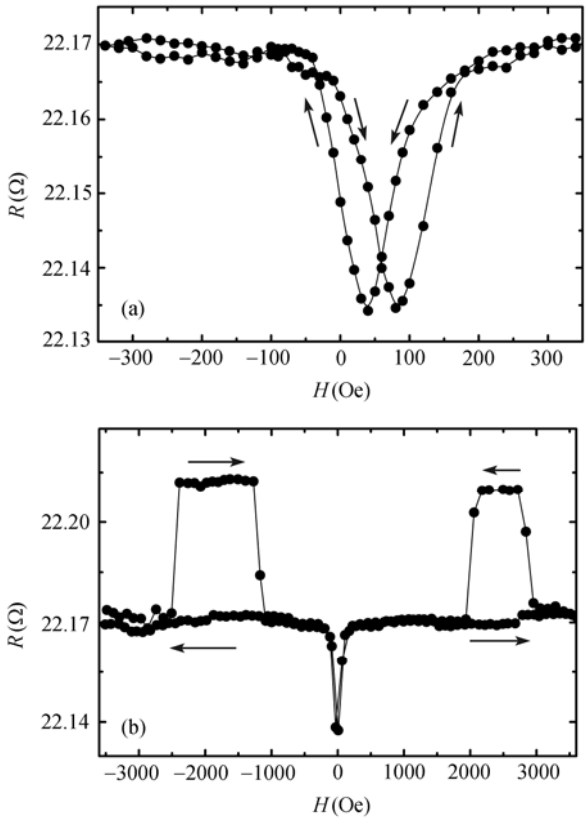

Figure 5 Resistance R of the Fe-oxide thin film as functions of external magnetic field H at room temperature.

low value due to antiparallel orientation of the moments. The positive MR sets in naturally since Fe in the core has a positive spin polarization and Fe_3O_4 in the shell a negative one[18,19].

It is also found that the minimum value of the resistance in the R-H loop at low field deviates from zero field, suggesting the appearance of an exchange field H_{ex} (about 50 Oe in this case). The origin of H_{ex} may be due to the shell-type column morphology where the oxide coating is believed to interact strongly with the Fe core[11]. The displacement is a consequence of the exchange anisotropy between the ferromagnetic Fe in the core and the iron oxides in the shell, which is also found in other ion-ion oxide coupled systems[12,20−22].

Compared to the patterned sample, a shift of the loop, ~4.9 Oe, is experienced for the unpatterned sample (see Figure 4). Such differences between them may come from the patterning process. Hu et al.[23] have verified that the H_c of Fe_3O_4 increases much after patterning. Bowen et al.[24] also found that optimizing the patterning process for $La_{2/3}Sr_{1/3}MnO_3/SrTiO_3/La_{2/3}Sr_{1/3}MnO_3$ oxide heterostructures could highly improve the MR effect.

Further studies are underway to understand this nature in such a system.

In contrast to the positive MR effect, a negative MR ratio in the large magnetic field range of $H > 1$ kOe is detected as shown in Figure 5(b). In the negative MR effect, the resistance is higher when the magnetizations of two electrodes are antiparallel to each other, corresponding to an increase of the resistance in the *R-H* curve. So the negative MR effect at large field may be identified with that in the case of the conventional tunneling systems[25], which originates from the magnetization switching between the shell-type columns[11,26] with the grain boundaries between columns acting as tunneling barriers.

Figure 6 shows the room-temperature *I-V* characteristic of the sample, in which there are Ohmic behavior at low electric fields and deviation from Ohm's law at high fields. It is reported that there are a few causes for the nonlinear *I-V* curve, i.e., intergrain tunneling[27] or inelastic hopping through tunneling barrier[28]. The non-Ohmic character of the resistance supports the present tunneling-type conduction between Fe-core and oxide-shell[29], and is responsible for the MR in the Fe-oxide thin films.

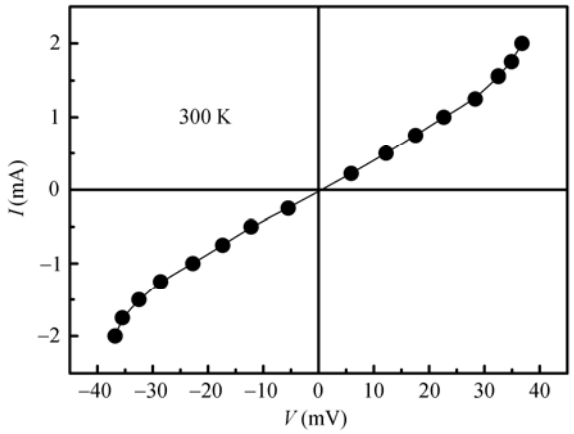

Figure 6 The *I-V* characteristic of the Fe-oxide thin film at 300 K.

For a better insight into the tunneling transport nature, ultraviolet (UV) photovoltaic effect of the sample was studied. Since the Fe-oxide film consists of columnar grains with the interface between the Fe-core and oxide-shell as a barrier, there is a chemical potential shift $\Delta\mu$ between the core and shell. Thus might induce a depletion layer in the boundary region, and the build-in voltage V_b is given by $\Delta\mu$, $V_b = \Delta\mu$. When the UV laser, which has a photon energy higher than the energy gap for Fe-oxide between occupied and empty electronic states, irradiates the sample, electron-hole pairs can be excited in the grains and boundary regions. And then the nonequilibrium carriers can be separated by the built-in electric field near the boundaries, eventually, leading to the appearance of an instant photovoltage. Figure 7 presents a typical photovoltage transient of the Fe-oxide thin film to a pulsed laser irradiation of 308 nm and 25 ns in duration, and confirms the above discussion. The energy density is 0.5 mJ/mm^2 and the irradiated area is 5×5 mm^2. The pulse response was monitored with a 500 MHz sampling oscilloscope terminated into 1 MΩ. The photovoltaic response shows a 10%—90% rise time of ~20 ns, which is limited by the excitation laser, and a full width for half maximum of 50 ns, suggestive of the lifetime of 50 ns for the nonequilibrium photo-induced carriers.

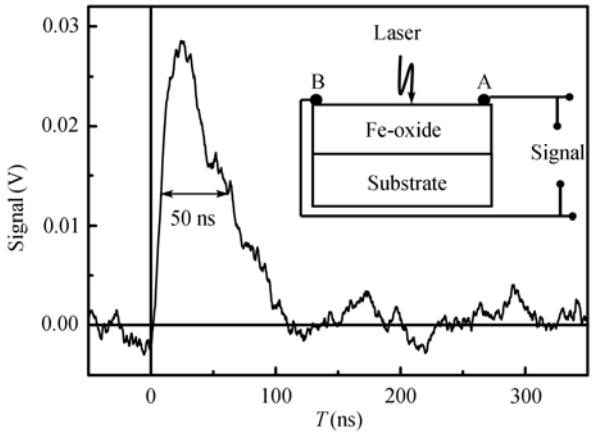

Figure 7 The open-circuit photovoltaic signal of the Fe-oxide film irradiated by a 308 nm laser pulse of 25 ns duration. The inset shows a schematic circuit of the sample measurement. Here, A and B denote the electrodes.

As shown in Figure 5, the magnitude of MR is much lower in spite of the high spin polarizations of magnetite and iron. The majority of numerous experimental realizations of tunneling MR displayed a very small low-field MR response[30]. The distorted or hard magnetic structure and decreased spin polarization were often suggested as possible reasons for the low value of low-field MR[30−33]. Almost any kind of magnetic reconstruction will mix the opposite spin states for magnetite as half metal, decreasing the local spin polarization and hence the MR. Since magnetotunneling is an interface effect, spin flip processes at the boundaries containing impurities and defects would certainly have a

deleterious effect on the MR.

3 Conclusion

In summary, we have observed the low-field positive and high-field negative MR at room temperature in multiphase Fe-oxide thin films. Based on the measurements of XRD, XPS and HRTEM, the morphology with the shell of Fe-oxide enclosing the Fe core was confirmed. The coexistence of positive and negative MRs is attributed to the tunneling-type conduction, which is further supported by the non-Ohmic character of the resistance and UV photovoltaic effect.

The authors would like to thank Professor Zhang Ze for his assistance in sample preparation.

1 Velikov K P, Moroz A, van Blaaderen A. Photonic crystals of core-shell colloidal particles. Appl Phys Lett, 2002, 80: 49—51
2 Zhou H, Alves H, Hofmann D M, et al. Behind the weak excitonic emission of ZnO quantum dots: ZnO/Zn(OH)$_2$ core-shell structure. Appl Phys Lett, 2002, 80: 210－212
3 Cao L X, Zhang J H, Ren S L, et al. Luminescence enhancement of core-shell ZnS:Mn/ZnS nanoparticles. Appl Phys Lett, 2002, 80: 4300－4302
4 Ebenstein Y, Mokari T, Banin U. Fluorescence quantum yield of CdSe/ZnS nanocrystals investigated by correlated atomic-force and single-particle fluorescence microscopy. Appl Phys Lett, 2002, 80: 4033－4035
5 Lauhon L J, Gudiksen M S, Wang C L, et al. Epitaxial core-shell and core-multishell nanowire heterostructures. Nature, 2002, 420: 57－61
6 Jackson J B, Westcott S L, Hirsch L R, et al. Controlling the surface enhanced Raman effect via the nanoshell geometry. Appl Phys Lett, 2003, 82: 257－259
7 Zeng H, Sun S H, Li J, et al. Tailoring magnetic properties of core/shell nanoparticles. Appl Phys Lett, 2004, 85: 792－794
8 Rossi G, Rapallo A, Mottet C, et al. Magic polyicosahedral core-shell clusters. Phys Rev Lett, 2004, 93: 105503
9 Noborisaka J, Motohisa J, Hara S, et al. Fabrication and characterization of freestanding GaAs/AlGaAs core-shell nanowires and AlGaAs nanotubes by using selective-area metalorganic vapor phase epitaxy. Appl Phys Lett, 2005, 87: 093109
10 Bauerecker S. Self-diffusion in core-shell composite $^{12}CO_2/^{13}CO_2$ nanoparticles. Phys Rev Lett, 2005, 94: 033404
11 Gangopadhyay S, Hadjipanayis G C, Dale B, et al. Magnetic properties of ultrafine iron particles. Phys Rev B, 1992, 45: 9778－9787
12 Prados C, Multigner M, Hemando A, et al. Dependence of exchange anisotropy and coercivity on the Fe-oxide structure in oxygen-passivated Fe nanoparticles. J Appl Phys, 1999, 85: 6118－6120
13 Rybchenko S I, Fujishio Y, Takagi H, et al. Effect of interface passivation on the magnetoresistance of granular magnetite $Fe_{3(1-\delta)}O_4$. Appl Phys Lett, 2006, 89: 132509
14 Zhao K, Feng J F, Huang Y H, et al. Magnetic field dependence of voltage-current characteristics of Fe_3O_4 thin films at room temperature. Appl Phys Lett, 2006, 88: 052506
15 Zhao K, Zhang L, Li H, et al. Magnetic coupling in La–Ca–Mn–O/La–Sr–Co–O/La–Ca–Mn–O sandwiches. J Appl Phys, 2004, 95: 7363－7365
16 Zhao K, Wong H K. Epitaxial growth of platinum thin films on various substrates by facing-target sputtering. J Crys Growth, 2003, 256: 283－287
17 Bennett K H, Della Torre E. Analysis of wasp-waist hysteresis loops. J Appl Phys, 2005, 97: 10E502
18 Yanase A, Siratori K. Band structure in the high temperature phase of Fe_3O_4. J Phys Soc Jpn, 1984, 53: 312－317
19 Zhang Z, Satpathy S. Electron states, magnetism, and the Verwey transition in magnetite. Phys Rev B, 1991, 44: 13319－13331
20 Ruf R R, Gambino R J. Iron-iron oxide layer films. J Appl Phys, 1984, 55: 2628－2630
21 Dimitrov D V, Murthy A S, Hadjipanayis G C, et al. Magnetic properties of exchange-coupled Fe/FeO bilayers. J Appl Phys, 1996, 79: 5106－5108
22 Del B L, Hernando A, Multigner M, et al. Evidence of spin disorder at the surface–core interface of oxygen passivated Fe nanoparticles. J Appl Phys, 1998, 84: 2189－2192
23 Hu G, Suzuki Y. Negative spin polarization of Fe_3O_4 in magnetite/manganite-based junctions. Phys Rev Lett, 2002, 89: 276601
24 Bowen M, Bibes M, Barthélémy A, et al. Nearly total spin polarization in $La_{2/3}Sr_{1/3}MnO_3$ from tunneling experiments. Appl Phys Lett, 2003, 82: 233－235
25 Li X W, Gupta A, Xiao G, et al. Fabrication and properties of heteroepitaxial magnetite (Fe_3O_4) tunnel junctions. Appl Phys Lett, 1998, 73: 3282－3284
26 Papaefthymiou V, Kostikas A, Simopoulos A, et al. Magnetic hysteresis and Mössbauer studies in ultrafine iron particles. J Appl Phys, 1990, 67: 4487－4489
27 Xu Y, Ephron D, Beasley M R. Directed inelastic hopping of electrons through metal-insulator-metal tunnel junctions. Phys Rev B, 1995, 52: 2843－2859
28 Neugebauer C A, Webb M B. Electrical conduction mechanism in ultrathin, evaporated metal films. J Appl Phys, 1962, 33: 74－82
29 Simmons J G. Generalized formula for the electric tunnel effect between similar electrodes separated by a thin insulating film. J Appl Phys, 1963, 34: 1793－1803
30 Ziese M. Extrinsic magnetotransport phenomena in ferromagnetic oxides. Rep Prog Phys, 2002, 65: 143－249
31 Rybchenko S I, Fujishio Y, Takagi H, et al. Effect of grain boundaries on the magnetoresistance of magnetite. Phys Rev B, 2005, 72: 054424
32 Srintiwarawong C, Gehring G A. Tunnelling from Fe_3O_4. J Phys Condens Matter, 2001, 13: 7987－7998
33 Dowben P A, Skomski R. Are half-metallic ferromagnets half metals? J Appl Phys, 2004, 95: 7453－7458